

Scatter Degradation and Correction Models for High-Resolution PET

Implicit in all scatter correction models in radioisotope imaging is the existence of some complementary degradation model describing the nature and processes giving rise to the measured scattered events. The general lack of theoretical connection between the degradation and correction models raises several important questions about the status and the fate of scattered events, and the formulation of the required scatter correction models. For instance, the question of whether scattered photons should be *reformed* or *removed* from society was recently raised by Links (1). This question is expected to become of paramount importance in very high-resolution PET in which the scatter degradation features become more complex (2-4). The aim of this article is to present alternative models for the degradation and scatter correction to bridge the gap between the degrading processes and the correction methods.

For the sake of simplicity, a high-resolution PET system will be considered to have two components in *series*: the object and detection subsystems, as shown in Figure 1. The response of each subsystem *i* to a line (point) source of unit radioactivity is assumed to have geometric (h_{ig}) and scatter (h_{is}) channels in *parallel*, which transmit unscattered and scattered photons, respectively. Since the imaging system is made of two (or more) such subsystems in series, the measured projection p_m is the result of a mixed channel process. The choice to reform or remove scattered photons emerging from each subsystem determines the normalization of the subsystem response which, in turn, determines which photons form the *ideal projection* at the input and dictates the fate of undesired components in the measured projection. As a rule, the intensity of the component(s) to be preserved for image formation in each subsystem is normalized to unity. Figure 1 illustrates several possible degradation models that are the basis of the scatter correction schemes described below.

In the deconvolution-restoration (DR) model (5), the useful component is assumed to be formed by both annihilation and scattered photons. Therefore, the response of each subsystem to a unit source

is normalized to unity and the ideal projection t is formed by a mixture of the annihilation and scattered photons subsequently transmitted through the object and detection subsystems. This ideal projection is blurred by convolution (*) to produce the measured projection:

$$p_m = t * h$$

$$= t * (h_{og} + h_{os}) * (h_{dg} + h_{ds}), \quad \text{Eq. 1}$$

where the subscripts *o* and *d* stand for the object and the detection subsystems, respectively. Since the annihilation photons transmitted through the object are not degraded by blurring, h_{og} is simply a delta function weighted by a scatter degradation factor which accounts for the loss of annihilation photons by scattering in the object (6):

$$h_{og} = (1 - f_o)\delta, \quad \text{Eq. 2}$$

where f_o is the relative intensity of object scatter or ratio of object scattered to total photons transmitted through the system. Expanding Eq. 1 and rearranging terms, we have:

$$p_m = t * \{(1 - f_o)h_{dg} + (1 - f_o)h_{ds} + h_{os} * (h_{dg} + h_{ds})\}$$

$$= t * \{h_g + h_d + h_o\}, \quad \text{Eq. 3}$$

where the imaging system's response $h = h_g + h_d + h_o$ is the sum of geometric (h_g), detector scatter (h_d) and object scatter (h_o) components. Since the object and detector subsystem responses (Eq. 1) are each normalized to unity, the measured response h of the overall system is automatically normalized to unity ($f_g + f_d + f_o = 1$). The scatter response functions h_d and h_o are respectively equivalent to the so-called scatter kernels F_o and F_d defined previously (2). The ideal projection t can be obtained by inversion of Equation 3 in the Fourier space (1):

$$T = P_m/H = P_m/(H_g + H_d + H_o). \quad \text{Eq. 4}$$

In this model, all counts are preserved since $1/H = 1$ at zero frequency. At higher frequencies, the deconvolution filter $1/H$ removes the blurring effects due to intrinsic resolution (H_g), detector scatter (H_d) and object scatter (H_o).

Conservation of all types of scattered events for image formation is attractive in many respects: images reconstructed from the restored projections, free of blurring,

have improved contrast, resolution and recovery coefficients (5); preservation of scatter increases the number of counts, thereby producing images with less statistical fluctuations; and when h is symmetric, H and the imaging system's modulation transfer function (MTF) can be used interchangeably. Because of such benefits, development of methods which reposition scattered photons to their original emission sites is a current research topic (5-7).

However, preserving scattered events in the image also has some drawbacks. It is not clear how restoration of the object scatter contributes to image sharpness since this component is confined to the low frequencies. As a result, its inclusion would actually reduce resolution since the inverse (Eq. 4) usually requires a narrower low-pass filter than when object scatter is excluded to suppress high frequency noise amplification. The inclusion of object scatter in images also complicates attenuation correction. Thus, it would be imprudent to minimize the minor effects of blurring at the expense of more important effects which undermine accuracy when quantitation is the primary objective. In view of these limitations, scatter removal has been considered as an alternative since attenuation correction is simplified while contrast and quantitation accuracy are improved (2,6,8,9).

The scatter convolution-subtraction (CS) model most commonly used for PET is based on approximations which make scatter removal possible without the recourse of low-pass filtering or shift-invariant response functions (8). Since scatter is unwanted, the ideal projection t' is assumed to be formed only by the annihilation (true) photons which are transmitted through the object and detection subsystems without undergoing Compton interactions. As before, the blurring effects are described by convolution:

$$p_m = t' * h'$$

$$= t' * (h'_{og} + h'_{os}) * (h'_{dg} + h'_{ds}). \quad \text{Eq. 5}$$

However, since only the geometric channels h'_{og} and h'_{dg} transmit the desired photons for image formation, each of these distributions are now normalized to unity. As the object subsystem does not modify the number and distribution of the annihilation photons, h'_{og} is simply the delta function (δ). Expanding Eq. 5 and rearranging terms, we get:

Received Aug. 21, 1995; revision accepted Feb. 7, 1996.

For correspondence or reprints contact: Roger Lecomte, PhD, Department of Nuclear Medicine and Radiobiology, University of Sherbrooke, Sherbrooke, Québec, Canada J1H 5N4.

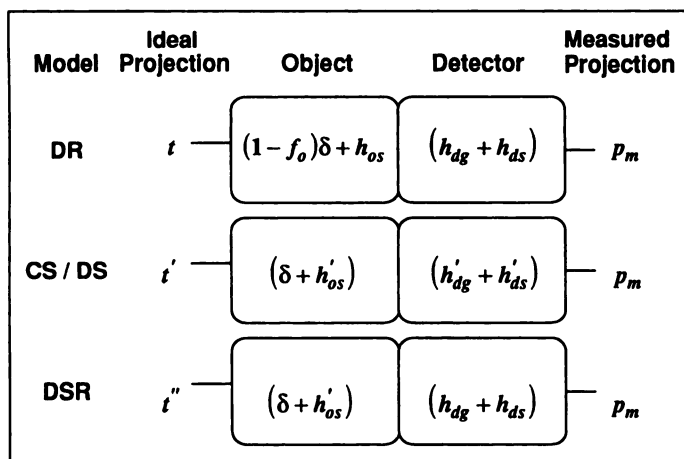


FIGURE 1. Response functions of the degradation models for object (o) and detector (d) subsystems in series. Each subsystem has a geometric (g) and a scatter (s) channel in parallel. The overall response to the ideal projection t , t' or t'' produces the measured projection p_m .

$$\begin{aligned}
 h' &= h'_{dg} + h'_{ds} + h'_{os} * (h'_{dg} + h'_{ds}) \\
 &= \frac{h_g}{f_g} + \frac{h_d}{f_g} + \frac{h_o}{f_g} \\
 &= \frac{h}{f_g}.
 \end{aligned}
 \tag{Eq. 6}$$

As before, the imaging system's response is the sum of geometric, detector scatter and object scatter components, but its intensity has been raised by the factor $1/(1 - f_o) = 1/f_g$. After computing Equation 6, the measured projection p_m can be expressed as the sum of three independent components

$$\begin{aligned}
 p_m &= t' * \frac{h_g}{f_g} + t' * \frac{h_d}{f_g} + t' * \frac{h_o}{f_g} \\
 &= p_{od} + s_d + s_o
 \end{aligned}
 \tag{Eq. 7}$$

and the scatter-free projection p_{od} is simply obtained by direct subtraction of the scatter contributions:

$$\begin{aligned}
 p_{od} &= p_m - s_o - s_d \\
 &= p_m - t' * \frac{h_o}{f_g} - t' * \frac{h_d}{f_g}.
 \end{aligned}
 \tag{Eq. 8}$$

Since the ideal projection t' is not known a priori, one might just approximate $s_i = t' * h_i/f_g$ by $s_i \approx p_m * h_i$ ($\delta, 10$) and expand the equation to separately subtract the scatter contributions, as suggested by Links (1):

$$\begin{aligned}
 p_{od} &= p_m - p_m * h_o - p_m * h_d \\
 &= p_m * (\delta - h_o - h_d).
 \end{aligned}
 \tag{Eq. 9}$$

However, this approach would be inconsistent with the formulation of the model since the detector scatter in Equation 6 does not have any dependence on the object subsystem and, therefore, it should not be estimated from the measured projection which includes the degradation effects of the object subsystem. To overcome this difficulty, the object scatter-free projections p_o must first be obtained by convolution-subtraction

ter-free projections p_o must first be obtained by convolution-subtraction

$$p_o = p_m - s_o = p_m * (\delta - h_o), \tag{Eq. 10}$$

to remove all events formed by photons which pass through the h'_{os} channel. One can then proceed to remove the detector scatter using similar approximations to estimate s_d by $p_o * h'_d/(1 - f_o)$, where the factor $1/(1 - f_o)$ is required to normalize the detector scatter response to the intensity of a line source in air (without the object). This reasoning leads to the desired result:

$$\begin{aligned}
 p_{od} &= p_o - s_d \\
 &= \{p_m * (\delta - h_o)\} * (\delta - h'_d/(1 - f_o)).
 \end{aligned}
 \tag{Eq. 11}$$

According to Equation 11, the CS model seeks to obtain the scatter-free distribution p_{od} , which is still blurred by the finite resolution of the detection subsystem, instead of the ideal projection t' .

To overcome this limitation, as well as the need to use the measured projection p_m as an input in estimating the scatter contributions, the deconvolution-subtraction (DS) model can be used. In this model, the ideal projection is defined as in the previous CS model and, therefore, Equations 5-7 are common to both the CS and DS models. The ideal projection is obtained by Fourier transforming Equation 7 and inverting the result:

$$T' = p_m/H' = p_m / \left(\frac{H_g}{f_g} + \frac{H_d}{f_g} + \frac{H_o}{f_g} \right). \tag{Eq. 12}$$

The subtraction capability of this model is derived from the fact that the intensities of the scatter components in Equation 6 are in excess of unity. Therefore, the inverse filter $1/H'$ at zero frequency is less than unity by a scaling factor f_g which effectively removes the object and detector scattered

events in the measured projections P_m to yield the scatter-free projection P_{od} . At higher frequencies, H_d and H_o in the deconvolution filter $1/H'$ remove the blurring effects of scattered events while H_g restores resolution to produce the desired ideal projection T' in the Fourier space.

In our accompanying article in this issue, we have shown that the benefits of removing s_d are only marginal in terms of image contrast, and are obtained at the expense of a substantial loss of scattered events which reasonably resolve the source. Such events could be included in image formation (2). To incorporate preferential treatment of selected scatter components, we propose a deconvolution-subtraction-restoration (DSR) model in which object and detector scatter are segregated as undesirable and useful events, respectively. In this case, the responses of the object and detection subsystems will be derived from the DS and DR models, respectively (Fig. 1). The ideal projection t'' is then formed by all annihilation photons transmitted through the object. Reformation is required to correct for their slight misplacement in the detector subsystem due to Compton scattering and finite intrinsic resolution. The degradation process producing the measured projection is then given by:

$$\begin{aligned}
 p_m &= t'' * h'' \\
 &= t'' * (\delta + h'_{os}) * (h_{dg} + h_{ds}) \\
 &= t'' * \{h_{dg} + h_{ds} + h'_{os} * (h_{dg} + h_{ds})\} \\
 &= t'' * \left\{ \frac{h_g}{f_g + f_d} + \frac{h_d}{f_g + f_d} + \frac{h_o}{f_g + f_d} \right\} \\
 &= t'' * \frac{h}{f_g + f_d}.
 \end{aligned}
 \tag{Eq. 13}$$

Solving for t'' in the frequency domain, the DSR model yields:

$$T'' = p_m / \left(\frac{H_g}{f_g + f_d} + \frac{H_d}{f_g + f_d} + \frac{H_o}{f_g + f_d} \right). \tag{Eq. 14}$$

Again, since the intensity of object scatter is in excess of unity in h'' , the inverse filter $1/H''$, scaled down by a factor $1/(f_g + f_d) = 1/(1 - f_o)$, effectively removes object scatter from the measured projection as it corrects for the blurring effects of intrinsic resolution and detector scatter at higher frequencies.

As mentioned before, the deconvolution models have two drawbacks in common. First, corrections performed in the frequency space require symmetric and shift-invariant response functions. The nonstationarity of the object scatter response can be fulfilled by estimating p_o by convolution-subtraction as described in Equation 10. The nonstationarity of the geometric

and detector scatter responses can be partially inscribed in the models using singular-value decomposition (11) or piecewise Fourier inversion (12). Second, the presence of the geometric component in the inverse requires a low-pass filter to suppress noise at high frequency. To overcome this limitation, a tradeoff between noise amplification and resolution loss can be made by setting the geometric component in the inverse filter to a constant value equal to its intensity. This enables one to omit the low-pass filter, since the inverse converges to this value at high frequency. In so doing, the scatter-corrected projections, unrestored for the intrinsic detector resolution, become in the different models:

$$\text{DR: } P_{\text{od}} = P_m / \{f_g + H_d + H_o\} \quad \text{Eq. 15a}$$

$$\text{DS: } P'_{\text{od}} = P_m / \left\{ 1 + \frac{H_d + H_o}{f_g} \right\} \quad \text{Eq. 15b}$$

$$\text{DSR: } P''_{\text{od}} = P_m / \left\{ \frac{f_g + H_d + H_o}{f_g + f_d} \right\}. \quad \text{Eq. 15c}$$

When the detector scatter intensity is small, such as is the case for lower resolution PET systems, both the DS and DSR models become identical and reduce to the gener-

alized scatter correction method commonly used in single photon emission tomography (9). When the detector scatter spread is narrow, a low-pass filter may still be required in the DR and DSR models since the inverse converges to a constant value above unity at high frequency. The inclusion of detector scatter in the desired components for image formation (2) suggests that some fraction of the object scatter which may not be detrimental to image quality could, in principle, be included as well. Such a model would undoubtedly reconcile the imaging goals of both *reformists* and *purists* in nuclear medicine.

REFERENCES

1. Links JM. Scattered photons as "good counts gone bad:" are they reformable or should they be permanently removed from society? *J Nucl Med* 1995;36:130-132.
2. Bentourkia M, Msaki P, Cadorette J, Lecomte R. Assessment of scatter components in high resolution PET: correction by nonstationary convolution subtraction. *J Nucl Med* 1995;35:121-130.
3. Bentourkia M, Msaki P, Cadorette J, Lecomte R. Energy dependence of scatter components in multispectral PET imaging. *IEEE Trans Med Imag* 1995;14:138-145.
4. Thompson CJ, Picard Y. Two new strategies to increase the signal to noise ratio in positron volume imaging. *IEEE Trans Nucl Sci* 1993;40:956-961.
5. Links JM, Leal JP, Mueller-Gaertner HW, Wagner

HN. Improved positron emission tomography quantification by Fourier-based restoration filtering. *Eur J Nucl Med* 1992;19:925-932.

6. King MA, Coleman M, Penney BC, Glick SJ. Activity quantitation in SPECT: a study of prereconstruction Metz filtering and the use of the scatter degradation factor. *Med Phys* 1991;18:184-189.
7. Frey EC, Tsui BMW. A practical method for incorporating scatter in a projector-backprojector for accurate scatter compensation in SPECT. *IEEE Trans Nucl Sci* 1993;40:1107-1116.
8. Bergström M, Eriksson L, Bohm C, Blomqvist G, Litton J. Correction for scattered radiation in a ring detector positron camera by integral transformation of the projections. *J Comput Assist Tomogr* 1983;7:42-50.
9. Msaki P, Axelsson B, Dahl CM, Larsson SA. A generalized scatter correction method in SPECT using point scatter distribution functions. *J Nucl Med* 1987;28:1861-1869.
10. Msaki P, Erlandsson K, Svensson L, Nolstedt L. The convolution scatter subtraction hypothesis and its validity domain in radioisotope imaging. *Phys Med Biol* 1993;38:1359-1370.
11. Lewitt RM, Muehlelehner G, Karp J. Three-dimensional image reconstruction for PET by multi-slice rebinning and axial image filtering. *Phys Med Biol* 1994;39:321-339.
12. Bentourkia M, Msaki P, Cadorette J, Lecomte R. Nonstationary scatter subtraction-restoration in high resolution PET. *J Nucl Med* 1996;37:2040-2046.

P. Msaki

M. Bentourkia

R. Lecomte

University of Sherbrooke
Sherbrooke, Quebec, Canada

A Graphical Analysis Method to Estimate Blood-to-Tissue Transfer Constants for Tracers with Labeled Metabolites

David A. Mankoff, Anthony F. Shields, Michael M. Graham, Jeanne M. Link and Kenneth A. Krohn
Division of Nuclear Medicine, University of Washington, Seattle, Washington; Wayne State University and the Karmanos Cancer Institute, Detroit, Michigan

The Patlak graphical analysis technique is a popular tool for estimating blood-to-tissue transfer constants from multiple-time uptake data. Our objective was to extend this technique to tracers with labeled metabolites, the presence of which can cause errors in the standard Patlak analysis. **Methods:** Based on previously described formulations, we generalized the graphical technique for use under specific conditions. To test the extended graphical approach, we applied the method to both simulated and patient data using a preliminary compartmental model for the PET tumor proliferation marker, 2-[¹¹C]-thymidine. **Results:** When given conditions are met, a linear relationship exists between the normalized tissue activity (tissue activity/blood activity) and a new set of graphical analysis basis functions, including a new definition of normalized time, which takes the presence of labeled metabolites into account. Graphical estimations of the tumor thymidine incorporation rate for simulated data were accurate and showed close agreement to the results of detailed compartmental analysis. In patient studies, the graphical

and compartmental estimates showed good agreement but a somewhat poorer correlation than in the simulations. **Conclusion:** The extended graphical analysis approach provides an efficient method for estimating blood-tissue transfer constants for tracers with labeled metabolites.

Key Words: PET; modeling; carbon-11-thymidine; metabolites

J Nucl Med 1996; 37:2049-2057

Radiopharmaceutical imaging is frequently complicated by the presence of labeled metabolites. The metabolites usually have a different distribution pattern than the parent tracer and can therefore cause errors in the kinetic analysis. When the blood concentrations of the tracer and its metabolites are known through blood sampling and metabolite analysis, tracer kinetic modeling can be used to separate the contributions of tracer and metabolites to the image and to estimate physiologic parameters based upon the tracer of interest. Models accounting for the behavior of the intact tracer and its metabolites are, by necessity, more complex and generally ill-suited for the routine estimation of physiologic parameters. In general, only the

Received May 22, 1995; revision accepted Feb. 28, 1996.

For correspondence or reprints contact: David A. Mankoff, MD, PhD, Division of Nuclear Medicine, Box 356113, University of Washington Medical Center, 1959 NE Pacific St., Seattle, WA 98195.